CrystEngComm

Accepted Manuscript

ROYAL SOCIETY OF CHEMISTRY

www.rsc.org/crystengcomm

Journal Name

COMMUNICATION

High-Energy Organic Groups Induced Spectrally Pure Upconversion Emission in Novel Zirconate-/Hafnate-based Nanocrystals

Received 00th January 20xx,
Accepted 00th January 20xx

DOI: 10.1039/x0xx00000x

www.rsc.org/

Xiang-Hong He,[a,b] Bing Yan*[a]

Lanthanide ions generally have abundant meta-stable excited states enabling lanthanide-doped nanocrystals (NCs) to display multipeak emission profiles. We address this issue by presenting a series of novel fluorides based nanophosphors exhibiting spectrally pure upconversion (UC) red fluorescence upon near-infrared (980 nm) excitation. Single-band deep-red UC luminescence was achieved when Yb^{3+}-Er^{3+} ion-pair was incorporated into K_3MF_7 (M = Zr, Hf). This UC luminescence feature of K_3MF_7:Yb^{3+},Er^{3+} (M = Zr, Hf) NCs is independent of the doping levels of Yb^{3+}-Er^{3+} and pump power of incident light. High-energy vibrational oscillators on the NCs surfaces are likely to result in the striking increase in the population of $^4F_{9/2}$ level of Er^{3+}, accounting for spectrally pure luminescence. The composition-optimized nanophosphor presents relatively perfect red monochromaticity.

Recently, lanthanide-doped upconversion (UC) nanoparticles have evoked considerable interest due to their unique properties including multicolor emission, large anti-Stokes shift, narrow emission bandwidth, high resistance to optical blinking and photobleaching, as well as low toxicity and deep tissue penetration depths (up to 10 mm) under exposure of NIR light (980 nm), which make them to be expected to have potential applications.[1,2] Despite the above gains, improvements are still needed to optimize optical properties for potential practical applications. A crucial aspect that needs improvement is the spectral purity of UC nanoparticles because the spectrally pure UC emission is beneficial for enhancing the precision and sensitivity of the indicators in fluorescent label detection.[2b,3] To date, several strategies have been developed to achieve spectral pure upconverted emission such as transition metal ions doping, [4] cross relaxation effect based on activator interaction,[5] and the combination of appropriate matrix with ion-pair as well as modification by means of surface organic group. Among them, it is believed that an excellent measurement is to combine lanthanide ions with fluoride hosts typically owing appropriate phonon energy.[6-7] Nevertheless, ladder-like system of energy levels in lanthanide ions typically leads to multiple emission peaks.[1a,8] To make up for this deficiency, wise choice of hosts is considered to be the most effective way to achieve single-band UC emission.[9] Unfortunately, suitable host materials meeting that above requirement are only restricted to some specific cases like $KMnF_3$, MnF_2, ZrO_2, $CaSc_2O_4$, ScOF and Na_3ZrF_7.[6, 9,10]

It is commonly believed that high-energy organic groups like OH usually act as primary centers of nonradiative transition. [11] To the best of our knowledge, spectrally pure upconversion luminescence induced by high-energy organic groups has been much less well explored. Herein, we aimed to investigate single-band UC emission properties of potassium heptafluo-zirconate/hafnate based nanocrystals (NCs). Pure and Yb^{3+}-Er^{3+} co-doped K_3MF_7(M = Zr, Hf) NCs were successfully prepared via a room-temperature complex procedure using oleic acid as chelating agent. Impressively, the presence of high-energy vibrational oscillators on the surfaces of NCs leads to the striking increase of population for $^4F_{9/2}$ level of Er^{3+}, giving rise to spectrally pure luminescence.

Experimental Section

Materials. All chemicals were of analytical grade and were used as received without further purification. Analytical grade rare earths oxides (Yb_2O_3, Er_2O_3, 99.99%), $ZrOCl_2{\cdot}8H_2O$ (≥ 99.0%), $HfOCl_2{\cdot}8H_2O$ (≥ 98.0%), $KF{\cdot}2H_2O$ (≥ 99.0%), NH_4F (≥ 96.0%), concentrated nitric acid (HNO_3, ≥ 68.0%), ethanol (≥ 99.7%), and cyclohexane (≥ 99.5%) were purchased from Sinopharm Chemical Reagent Co., China. Rare earths oxides were separately dissolved in dilute HNO_3 solution and the residual HNO_3 was removed by heating and evaporation, resulting in the formation of aqueous solution of corresponding $RE(NO_3)_3$. Oleic acid (OA), potassium oleate (KOA), and oleylamine (OM) were supplied by Alfa Aesar Co., China.

Synthesis. Pure and lanthanide-doped K_3MF_7 (M = Zr, Hf) NCs were prepared via a solution-phase complex chemical method at room-temperature (25 ℃). Herein we took the synthesis of K_3ZrF_7 NCs as

a Department of Chemistry, Tongji University, Siping Road 1239, Shanghai 200092, China.E-mail: byan@tongji.edu.cn
b School of Chemistry and Environmental Engineering, Jiangsu University of Technology, Changzhou 213001, China
†Electronic Supplementary Information (ESI) available. SeeDOI:10.1039/b000000x/

an example. In a typical preparation, KOA (0.5 mmol, 2.62 g), 5.0 mL OM, and 20.00 g oleic acid were mixed together in a plastic beaker under stirring at room-temperature, followed by the addition of 40.00 mL alcohol solution of $ZrOCl_2$ (12.5 mM). The mixture was stirred vigorously for 6 hours. Subsequently, the aqueous solution of KF (0.19 g) and NH_4F (4.00 mL, 1.00 M) was slowly added into the mixture. After continually stirring for 30 min, the mixture was left to stand for 12 hours at 25 ℃. The products were collected by centrifugation, washed sequentially with cyclohexane and ethanol for several times. After dried in a vacuum at room-temperature for 24 hours, K_3ZrF_7 powder was obtained. The synthetic procedure of lanthanide-doped K_3ZrF_7/K_3HfF_7 NCs was the same as that used to prepare K_3ZrF_7 host, except that the stoichiometric amounts of $ZrOCl_2$/$HfOCl_2$ and $Ln(NO_3)_3$ (Ln = Yb^{3+}/Er^{3+}) mixed solutions were added into the initial mixture.

Physical characterization. The crystallographic structure and phase purity were determined by powder X-ray diffraction (XRD) using a Bruker D8 Advanced X-ray diffractometer with Ni filtered Cu K_α radiation (λ = 1.5406 Å) at a voltage of 40 kV and a current of 40 mA. The morphology and chemical composition of the samples were characterized on a Hitachi S4800 field-emission scanning electron microscope (FE-SEM) equipped with an energy dispersive X-ray spectroscope (EDS). The photoluminescence properties were investigated in the solid state. Up-conversion fluorescence spectra were collected on an Edinburgh Instruments FLS920 phosphorimeter using a 980 nm laser diode (Module K98D08M-30mW, China) as excitation source. Fourier transform infrared (FT-IR) spectrum in transmission mode was measured on a Nicolet 5SXC FT-IR spectrophotometer using the KBr pellet technique. Raman backscattering measurements were performed using a Renishaw in via spectrophotometer equipped with an Olympus microscope, a liquid-N_2-cooled CCD detector, and an Ar^+ ion laser (λ = 514.5 nm, 30 mW) as the exciting source.

Results and Discussion

As shown in Figure 1, XRD patterns of K_3ZrF_7 and K_3HfF_7 samples exhibit sharp and intense peaks indicative of highly crystalline and can be well indexed as cubic K_3ZrF_7 (JCPDS no. 73-1530, space group Fm-3m), and cubic K_3HfF_7 (JCPDS no. 78-1827, space group *Fm-3m*), respectively. No trace of other characteristic peaks was observed for impurity phases. The calculated lattice constants are as follows: a = 8.951(1) Å for K_3ZrF_7, and a = 8.973(4) Å for K_3HfF_7, which is in good agreement with the corresponding standard values for the bulk cubic K_3MF_7 (M = Zr, Hf). In the lattice of both isostructural compounds K_3ZrF_7 and K_3HfF_7, $[MF_7]^{3-}$ pentagonal bipyramid (D_{5h}) species exist as isolated complex anions surrounded by K^+ ions.[12] The three-fold axis of $[MF_7]^{3-}$ can be oriented parallel to any of the eight [111] directions.[13] The nearst-neighbour F–F distances are 2.64 Å, which is slightly less than twice the ionic radius of fluorine (2.72 Å),[13a] and the average Zr–F distance is ~2.10 Å.[13] M^{4+} cations are coordinated to seven fluorine ions.[12a, 13] According to the Debye-Scherrer formula, the average crystallite sizes of K_3ZrF_7 and K_3HfF_7 NCs were estimated as ~69, and 87 nm, respectively, which matched well with the corresponding SEM observations. SEM images show that K_3ZrF_7 and K_3HfF_7 samples are quasi-spherical with a diameter ranging from 45 to 72 nm for K_3ZrF_7, 50 ~ 93 nm for K_3HfF_7 (Figure S1 in supporting information).

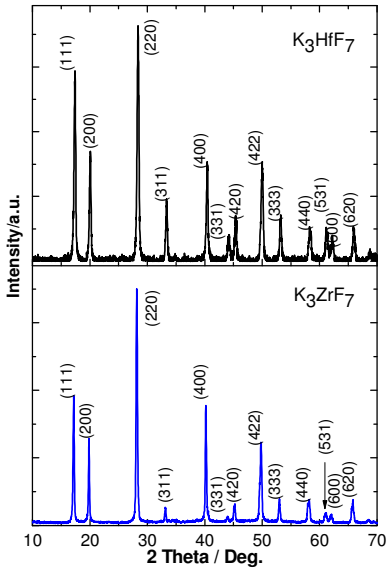

Figure 1 XRD patterns of as-obtained K_3ZrF_7 (bottom curve), and K_3HfF_7 (top curve) NCs (background uncorrected).

Since Yb^{3+}-Er^{3+} ion-pair can be easily incorporated into the K_3ZrF_7 or K_3HfF_7 lattices (phase and compositional analyses of Yb^{3+}-Er^{3+} codoped $K_3(Zr,Hf)F_7$ nanophosphors were given in Figures S2~S6 in supporting information), the as-obtained K_3MF_7 (M=Zr, Hf) NCs is strongly expected to be suitable UC hosts for Yb^{3+}-Er^{3+} in the view of structure characteristics. On the other hand, Raman spectra of K_3ZrF_7 and K_3HfF_7 samples are shown in Figure 2. The well-resolved sharp peaks indicated that all the samples were highly crystallized, which is in agreement with above XRD results. The strongest phonon mode is about 546 cm^{-1}, which is away from the frequency ranges of visible spectral region (1250–2500 cm^{-1}).[7a] More importantly, this photon frequency value is similar to those of calcium scandate (540 cm^{-1}) and sodium heptafluozirconate (556 cm^{-1}),[10d,14] which were found to present perfect green and red UC monochromaticity upon doping of Yb^{3+}-Ho^{3+} and Yb^{3+}-Er^{3+} ion-pairs, respectively.[6b,10d] Obviously, we believe that the as-prepared K_3MF_7 (M=Zr, Hf) can act as promising host lattices for efficient single-band emission. To validate this point, we investigated the UC properties of Yb^{3+}-Er^{3+} co-doped K_3MF_7 (M=Zr, Hf) in detail.

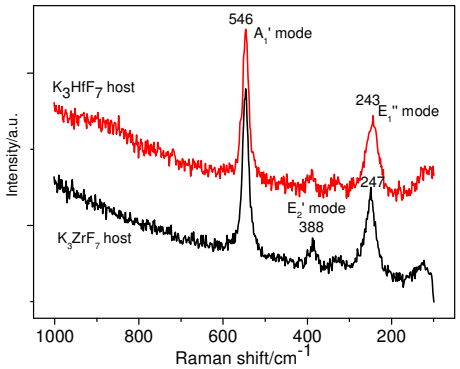

Figure 2 Raman spectra of K_3ZrF_7 and K_3HfF_7 hosts (the assignments of bands are also included).

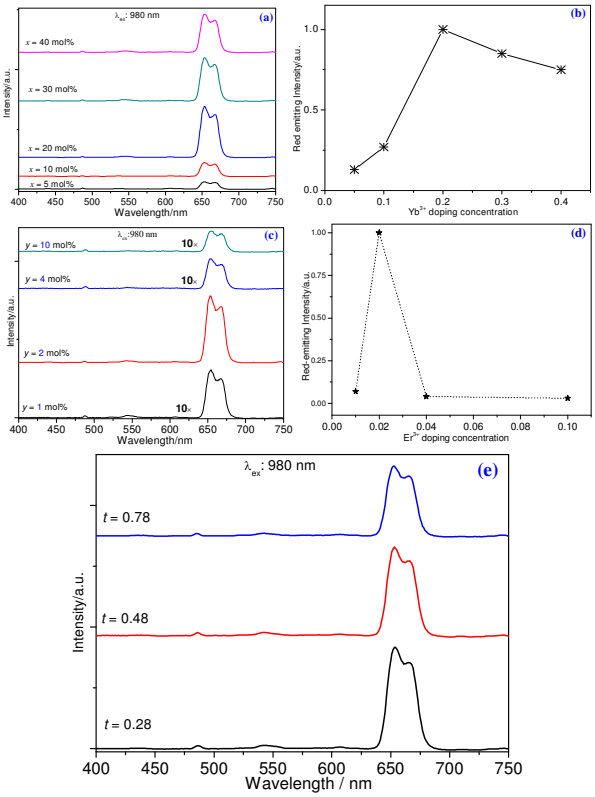

Figure 3 (a) UC emission spectra and (b) red-emitting intensity as a function of Yb^{3+} doping concentrations (*x* value) for K_3ZrF_7:Yb^{3+},Er^{3+}(*x*/2 mol%), (c) UC emission spectra and (d) red-emitting intensity as a function of Er^{3+} doping levels (*y* value) for K_3ZrF_7:Yb^{3+},Er^{3+}(20/*y* mol%) (The intensities of the samples with *y* values of 1 mol%, 4 mol%, and 10 mol% are magnified 10 times for the sake of comparison), (e) UC emission spectra of $K_3(Zr_{0.78-t}Hf_t)F_7$:Yb^{3+},Er^{3+}(20/2 mol%) samples with various contents of Hf^{4+}(*t* value).

Figures 3a and 3c depict UC emission spectra of Yb^{3+}-Er^{3+} co-activated K_3ZrF_7 NCs. In comparison with Yb^{3+}-Er^{3+} co-doped routine rare-earth-based fluorides NCs which typically exhibit multiple-band emissions in the visible spectral region,[15,16] a deep-red emission band ranging from 640 nm to 680 nm ($^4F_{9/2} \rightarrow {}^4I_{15/2}$ transition of Er^{3+}) for K_3ZrF_7:Yb^{3+},Er^{3+} was observed, while the green emission was almost restrained. The red emission band is composed of two main peaks, which results from the split of Er^{3+} $^4F_{9/2}$ generated by the crystal field.[6c] UC emission behavior as a function of Yb^{3+} or Er^{3+} doping concentrations was investigated (Figure 3b and 3d). Significantly, the single-band emission feature of K_3ZrF_7:Yb^{3+},Er^{3+} NCs remains the same on changing doping contents of Yb^{3+} (5–40 mol%) and Er^{3+} (1–10.0 mol%). As for K_3ZrF_7:Yb^{3+},Er^{3+}(*x*/2 mol%) samples with fixed level of Er^{3+}, the UC emission intensity enhances with increasing Yb^{3+} content from 5 to 20 mol% and then gradually weakens with further increasing Yb^{3+} level to 40 mol% (Figure 3 b). For K_3ZrF_7:Yb^{3+},Er^{3+}(20/*y* mol%) NCs, the optimal Er^{3+} doping level was determined to be 2.0 mol% (Figure 3d). As exhibited in Figure 3e, the single-band emission characteristics of $K_3(Zr_{0.78-t}Hf_t)F_7$:Yb^{3+},Er^{3+}(20/2 mol%, $0.28 \leq t \leq 0.78$) NCs is well maintained in all Hf^{4+}-modified samples.

All together, the above results suggest that single-band UC emission feature is independent of the doping levels of Yb^{3+}-Er^{3+} and the content of Hf^{4+} in host lattice. Similar phenomena were also observed in tetragonal Na_3ZrF_7:Yb^{3+},Er^{3+},[6b] and in Yb^{3+}-Er^{3+} co-doped Mn^{2+}-containing NCs such as $KMnF_3$ and MnF_2.[10b,10c]

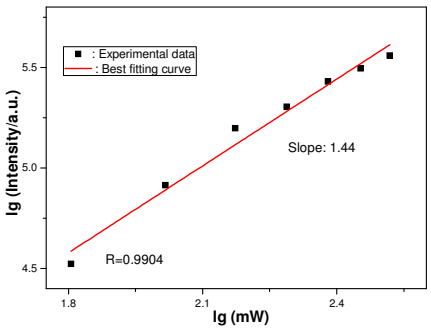

Figure 4 Pump power dependence of $^4F_{9/2} \rightarrow {}^4I_{15/2}$ emission intensity of Er^{3+} for K_3ZrF_7:Yb^{3+},Er^{3+}(20/2 mol%) NCs.

Firstly, we investigated UC emission intensity for $^4F_{9/2} \rightarrow {}^4I_{15/2}$ transition of Er^{3+} as a function of incident power. It is well known that the UC emission intensity (*I*) is proportional to the pump power of the pump power (*P*) for the UC process. A plot of lg*I* versus lg*P* yields a straight line with slope *n*.[17] As shown in Figure 4, based on the best fit with a power function, the slope is calculated to be 1.44. According to Pollnau *et al.*,[36] slope of the pump power dependence of UC emission intensity is determined by the competition between the UC and decay process in the intermediate level. Specifically, while UC is the dominant process which depopulates the intermediate levels, slope tends to a limit of 1, while decay is the dominant process, slope tends to 2. In our case, the observed slope is near to 1, indicating that the UC for K_3ZrF_7:Yb^{3+},Er^{3+} is mainly depopulation the intermediate levels.

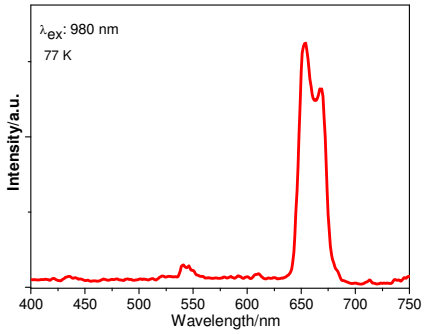

Figure 5 UC emission spectrum at 77 K of K_3ZrF_7:Yb^{3+},Er^{3+}(20/2 mol%) nanophosphor.

Likewise, at the low-temperature (77 K) Yb^{3+}-Er^{3+}-codoped K_3ZrF_7 NCs remained a single-band UC emission (Figure 5), indicating that the phonon participation in the transfer process has only a slight effect on the depopulation of the excited states.

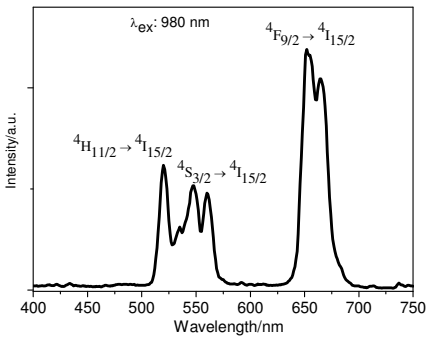

Figure 6 UC emission spectrum of K_3ZrF_7:Yb^{3+},Er^{3+}(20/2 mol%) sample annealed at 350 ℃.

In order to investigate the high-energy groups absorbed on the surface of NCs, the as-obtained K_3ZrF_7:Yb^{3+},Er^{3+}(20/2 mol%) NCs were annealed at 350 ℃ for 2 hrs. After then, the FT-IR (Figure S7) and UC (Figure 8) emission spectra of sample were measured. As exhibited in Figure S7, the stretching vibrations bands involving OH, CH_2 and COO groups disappeared, indicating the lack of high-energy organic groups. However, the green luminescence from $^4H_{11/2}\rightarrow{}^4I_{15/2}$ and $^4S_{3/2}\rightarrow{}^4I_{15/2}$ transitions of Er^{3+} in the sample calcinated at 350 ℃ was enhanced compared to that of as-obtained nanophosphor, which resulted in yellow emission rather than red fluorescence upon 980 nm excitation. (Figure 6) In this case, the corresponding CIE chromaticity coordinates were shifted to (x = 0.3648，y = 0.5615), located in the yellow light region. The variation of emission color suggested that the high-energy groups can greatly influence the decay of $^4I_{11/2}$ and $^4I_{13/2}$ intermediate states of Er^{3+}. $^4I_{11/2}$ and $^4I_{13/2}$ levels are the intermediate states responsible for green and red emissions, respectively.

Depopulation of an excited state may occur either via a direct transition to a lower lying state, which is radiative, or via a phonon-assisted transition, which is non-radiative (also referred to as non-radiative decay).[18] In the excited state of Er^{3+}, excited photon loss due to transfer of energy to the nearby surrounding phonons of high energy group is usually achieved via a multiphonon relaxation (MR).[8, 10a] The gap energies between $^4I_{11/2}$ and $^4I_{13/2}$ states and between $^4S_{3/2}$ and $^4F_{9/2}$ states of Er^{3+} are around 3600, and 3000 cm^{-1}, respectively. According to the following equations 1 and 2 (K is inversely proportional to the phonon numbers),

$$K = A\exp(-\beta g) \quad (1) \qquad g = \Delta E / \hbar\omega_m \quad (2)$$

where K is MR rate constant, A (in hertz) and β are constants, g is phonon numbers needed in the MR, ΔE stands for the energy gap to the next lower level, and $\hbar\omega_m$ is the phonon cutoff frequency.[19] Bridging the gap, using phonon energies of 546 cm^{-1}, is not very favorable due to the requirement for the availability of a large number of phonons (at least seven phonons).[18] As exhibited in Figure S8, the organic groups OH and CH_2 possess high-energy vibrational modes (2800-3600 cm^{-1}), in comparison with the dominant phonon modes in K_3ZrF_7 (546 cm^{-1}). $^4I_{11/2}$ level can easily decay to the lower level (energy gap ~3600 cm^{-1}) with the aim of high-energy organic groups such as OH and CH_2.[6c,8] In such case, $^4I_{11/2}$ level non-radiative decay to the lower-lying, intermediate level ($^4I_{13/2}$) occurs, leading to red emission. Hence, we believed that the single-band UC emission can be ascribed to the striking increase in the population of $^4F_{9/2}$ level reduced by high-energy organic groups on the surfaces of K_3ZrF_7:Yb^{3+},Er^{3+} NCs.

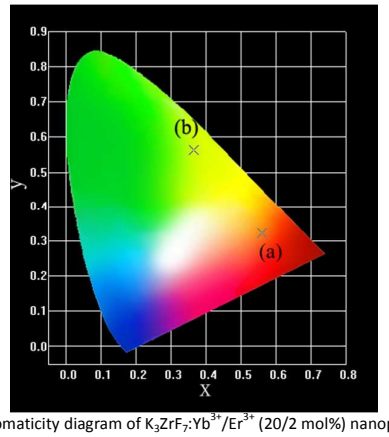

Figure 7 CIE chromaticity diagram of K_3ZrF_7:Yb^{3+}/Er^{3+} (20/2 mol%) nanophosohor before (a) and after (b) heat treated at 350 ℃.

As shown in Figures 3b and 3d, the strongest UC emission is realized for a 20/2 mol% Yb^{3+}/Er^{3+}-doping concentration. The Commission Internationale de L'Eclairage (CIE) chromaticity coordinates for the emission spectrum are calculated to be (x = 0.5846, y = 0.3227), located in the red light region (point **a** Figure 7). To evaluate the spectral purity quantificationally, Chan *et al.* recently introduced a parameter (S_{gr}), S_{gr} = $(A_g - A_r)/(A_g + A_r)$, where A_g and A_r are the integrated areas from 500 to 600 nm and from 600 to 700 nm, respectively.[9] S_{gr} varies from −1 to +1 with −1 (+1) corresponding to purely red (green) emission. According to this definition, S_{gr} value of K_3ZrF_7:Yb^{3+},Er^{3+}(20/2 mol%) nanophosphor is calculated as − 0.90, which is close to the highest value for $NaYF_4$:Er^{3+},Tm^{3+}(2/2 mol%) NCs with almost completely pure red emission (S_{gr} = − 0.95).[3d]

Conclusions

In summary, we have demonstrated for the first time the preparation and UC luminescent feature of single-phase potassium heptafluo-zirconate/hafnate NCs obtained by a simple complex chemical route under ambient conditions. Cubic K_3MF_7 (M = Zr, Hf) were found to be perfect host materials for efficient UC generation of lanthanides ions. Single-band UC luminescence under 980 nm excitation is achieved in Yb^{3+}-Er^{3+} co-doped K_3MF_7 (M = Zr, Hf) samples. The presence of high-energy vibrational oscillators on the surfaces of K_3ZrF_7: Yb^{3+},Er^{3+} NCs is likely to result in the striking increase in the population of $^4F_{9/2}$ level of Er^{3+}, giving rise to spectrally pure luminescence. The spectral purity was evaluated and the value found for composition-optimized K_3ZrF_7: Yb^{3+},Er^{3+} was S_{gr} = − 0.90, which is close to the highest value for $NaYF_4$:Er^{3+},Tm^{3+}(2/2 mol %) NCs achieved so far.

Acknowledgements

This work was supported by the National Natural Science Foundation of China (91122003), Developing Science Funds of Tongji University and the Science & Technology Commission of Shanghai Municipality (14DZ2261100).

Notes and references

1 (*a*) F. Auzel, *Chem. Rev.*, 2004, **104,** 139; (*b*) F. Wang and X. G. Liu, *Acc. Chem. Res.*, 2014, **47**, 1378; (*c*) J. Zhou, Z. Liu and F. Y. Li, *Chem. Soc. Rev.*, 2012, **41**, 1323; (*d*) S. L. Gai, C. X. Li, P. P. Yang and J. Lin, *Chem. Rev.*, 2014, **114**, 2343; (*e*) V. Muhr, S. Wilhelm, T. Hirsch and O. S. Wolfbeis, *Acc. Chem. Res.*, 2014, **47**, 3481; (*f*) C. X. Li and J. Lin, *J. Mater. Chem.*, 2010, **20**, 6831.

2 (*a*) H. H. Gorris and O. S. Wolfbeis, *Angew. Chem. Int. Ed.*, 2013, **52**, 3584; (*b*) Y. I. Park, J. H. Kim, K. T. Lee, K. S. Jeon, H. Bin Na, J. H. Yu, H. M. Kim, N. Lee, S. H. Choi, S. I. Baik, H. Kim, S. P. Park, B. J. Park, Y. W. Kim, S. H. Lee, S. Y. Yoon, I. C. Song, W. K. Moon, Y. D. Suh and T. Hyeon, *Adv. Mater.*, 2009, **21**, 4467; (*c*) Z. W. Wei, L. N. Sun, J. L. Liu, J. Z. Zhang, H. R. Yang, Y. Yang and L. Y. Shi, *Biomaterials*, 2014, **35**, 387; (*d*) X. Q. Ge, L. Dong, L. N. Sun, Z. M. Song, R. Y. Wei, L. Y. Shi and H. G. Chen, *Nanoscale*, 2015, **7**, 7206; (*e*) C. X. Li, J. Yang, Z. W. Quan, P. P. Yang, D. Y. Kong and J. Lin, *Chem. Mater.*, 2007, **19**, 4933;

(*f*) C. X. Li, Z. W. Quan, J. Yang, P. P. Yang and J. Lin, *Inorg. Chem.*, 2007, **46**, 6329

3 (*a*) F. Wang, D. Banerjee, Y. S. Liu, X. Y. Chen and X. G. Liu, *Analyst*, 2010, **135**, 1839; (*b*) M. J. Dejneka, A. Streltsov, S. Pal, A. G. Frutos, C. L. Powell, K. Yost, P. K. Yuen, U. Müller and J. Lahiri, *Proc. Natl. Acad. Sci. USA*, 2003, **100**, 389; (*c*) G. Y. Chen, Y. G. Zhang, G. Somesfalean, Z. G. Zhang, Q. Sun and F. P. Wang, *Appl. Phys. Lett.*, 2006, **89**, 163105; d) E. M. Chan, G. Han, J. D. Goldberg, D. J. Gargas, A. D. Ostrowski, P. J. Schuck, B. E. Cohen and D. J. Milliron, *Nano Lett*., 2012, **12**, 3839.

4 (*a*) G. Tian, Z. J. Gu, L. J. Zhou, W. Y. Yin, X. X. Liu, L. Yan, S. Jin, W. L. Ren, G. M. Xing and S. J. Li, *Adv. Mater.*, 2012, **24**, 1226; (*b*) S. J. Zeng, Z. G. Yi, C. Qian, H. B. Wang, J .Rao, T. M. Zeng, H. R. Liu, H. J. Liu and B. Fei, *Adv. Funct. Mater.*, 2014, **24**, 4051.

5 Wei W, Zhang Y, Chen R, J. L. Goggi, N. Ren, L. Huang, K. K. Bhakoo, H. D. Sun and T. T. Y. Tan. *Chem. Mater.*, 2014, **26**, 5183.

6 (*a*) Y. Liu, Q. Yang and C. Xu, *J. Appl. Phys*., 2008, **104**, 064701; (*b*) D. Q. Chen, L. Lei, R. Zhang, A. P. Yang, J. Xu and Y. S. Wang, *Chem. Commun.*, 2012, **48**, 10630; (*c*) L. Liu, Y. X. Wang, Y. F. Bai, X. R. Zhang, K. Yang, C. H. Huang and Y. L. Song, *Opt. Commun.*, 2012, **285**, 1528.

7 (*a*) R. Jia, Y. Liu, D. He, Q, Lü, G. Shan, Z. Liu, Y. Bai and T. Li, *Chem. J. Chin. Univ.*, 2004, **25**, 1306; (*b*) G. Chen, G. Somesfalean, Y. Liu, Z. Zhang, Q. Sun and F. Wang, *Phys. Rev. B*, 2007, **75**, 195204.

8 M. Haase and H. Schäfer, *Angew. Chem. Int. Ed.*, 2011, **50**, 5808.

9 Y. Wang, T. Wen, H. Zhang, J. Sun, M. Zhang, Y. Guo, W. Luo, M. Xia, Y. Wang and B. Yang, *J. Phys. Chem. C*, 2014, **118**, 10314.

10 (*a*) J. Zhao, Y. Sun, X. Kong, L. Tian, Y. Wang, L. Tu, J. Zhao and H. Zhang, *J. Phys. Chem. B*, 2008, **112**, 15666; (*b*) J. Wang, F. Wang, C. Wang, Z. Liu and X. G. Liu, *Angew. Chem. Int. Ed.*, 2011, **50**, 10369; (*c*) Z. Bai, H. Lin, J. Johnson, S. C. Rong Gui, K. Imakita, R. Montazami, M. Fujii and N. Hashemi, *J. Mater. Chem. C*, 2014, **2**, 1736; (*d*) J. Li, J. Zhang, Z. Hao, X. Zhang, J. Zhao and Y. Luo, *ChemPhysChem*, 2013, **14**, 4114.

11 M. Niraj Luwang, R. S. Ningthoujam, Jagannath, K. Srivastava and R. K. Vatsa, *J. Am. Chem. Soc.*, 2010, **132**, 2759.

12 (*a*) V. Dracopoulos, J. Vagelatos and G. N. Papatheodorou, *J. Chem. Soc. Dalton Trans.*, 2001, **7**, 1117; (*b*) M. Dova, M. Caracoche, A. Rodríguez, J. Martínez, P. Rivas, A. L. García and H. Viturro, *Phys. Rev. B*, 1989, **40**, 11258.

13 (*a*) G. C. Hampson and L. Pauling, *J. Am. Chem. Soc.*, 1938, **60**, 2702; (*b*) E. Reynhardt, J. Pratt, A. Watton and H. Petch, *J. Phys. C: Solid State Phys.*, 1981, **14**, 4701.

14 L. M. Toth, A. S. Quist and G. E. Boyd, *J. Phys. Chem.*, 1973, **77**, 1384.

15 (*a*) X. H. He and B. Yan, *J. Mater. Chem. C*, 2014, **2**, 2368; (*b*) D. Tu, Y. Liu, H. Zhu and X. Chen, *Chem. Eur. J.*, 2013, **19**, 5516; (*c*) H. H. Gorris and O. S. Wolfbeis, *Angew. Chem. Int. Ed.*, 2013, **52**, 3584.

16 (*a*) L. Liang, Y. Liu, C. Bu, K. Guo, W. Huang, T. Peng, B. Sebo, M. Pan, W. Liu, S. Guo, X. Z. Zhao, Dye Sensitized Solar Cells. *Adv. Mater.*, 2013, **25**, 2174; (*b*) J. C. Boyer, F. Vetrone, L. A. Cuccia, J. A. Capobianco, *J. Am. Chem. Soc.*, 2006, **128**, 7444.

17 (*a*) A. S. Oliveira, M. T. de Araujo, A. S. Gouveia-Neto, J. A. Medeiros Neto, A. S. B. Sombra and Y. Messaddeq, *Appl. Phys. Lett.*, 1998, **72**, 753; (*b*) M. Pollnau, D.R. Gamelin, S.R. Lüthi and M.P. Hehlen, *Phys. Rev. B*, 2000, **61**, 3337.

18 R. Naccache, Q. Yu and J. A. Capobianco, *Adv. Opt. Mater.*, 2015, **3**, 482.

19 J. M. F. Van Dijk and M. F. H. Schuurmans, *J. Chem. Phys.*, 1983, **78**, 5317.

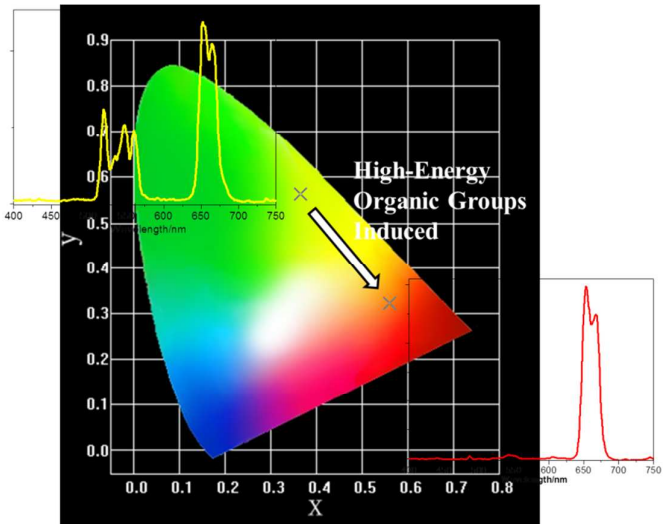

A series of novel fluorides based nanophosphors (NPs) exhibiting spectrally pure upconversion (UC) red fluorescence upon near-infrared (980 nm) excitation. Single-band deep-red UC luminescence feature of $K_3MF_7:Yb^{3+},Er^{3+}$ (M = Zr, Hf) NPs is independent of the doping levels of Yb^{3+}-Er^{3+} and pump power of incident light. High-energy vibrational oscillators on the NPs surfaces are likely to result in the striking increase in the population of $^4F_{9/2}$ level of Er^{3+}, accounting for spectrally pure luminescence.